Surface treatment of alumina ceramic for improved adhesion to a glass fibre-reinforced polyester composite

K.B. Lausund[1,2], B.B. Johnsen[1,*], D.B. Rahbek[1], F.K. Hansen[1,3]

[1] Norwegian Defence Research Establishment (FFI), P.O. Box 25, NO-2027 Kjeller, Norway
[2] Department of Physics, University of Oslo, P. O. Box 1048 Blindern, NO-0316 Oslo
[3] Department of Chemistry, University of Oslo, P.O. Box 1033 Blindern, NO-0315 Oslo, Norway
[*] Corresponding author. Tel.: +4763807834. E-mail address: bernt.johnsen@ffi.no (B.B. Johnsen).

ABSTRACT

The adhesion between an alumina ceramic and a glass fibre-reinforced polyester matrix composite has been investigated. The effect of various alumina surface treatments, including degreasing, etching, plasma, grit-blasting and silanisation, was evaluated. The physical and chemical surface properties were investigated by microscopy, profilometry, contact angle measurements and X-ray photoelectron spectroscopy. The analysis showed that the treatments removed organic contaminants from the alumina, resulting in higher surface free energies. Alumina/composite test specimens were prepared by a vacuum moulding technique, and the adhesive strength was evaluated using the fixed arm peel test. All surface treatments had a pronounced effect on the peel strength, and the adhesion was improved compared to the as-received alumina. This was verified by investigation of the fracture surfaces. The silane treatment produced a thin silane layer on the surface and had the greatest effect on the adhesive strength. This could be explained by the silane acting as an adhesion promoter between the alumina and the composite, better wetting of the more planar silane treated surface by the thermoplastic polyester, and a more defect-free alumina/polyester interphase.

Keywords
B. Surface treatment
B. Alumina
B. Composites
C. Peel
Surface analysis

DOI til publisert versjon / DOI to published version: 10.1016/j.ijadhadh.2015.07.015

1 Introduction

Protection against high-velocity impact from objects such as projectiles is a major issue in many military and also civilian applications. In many cases, hybrid armour systems consisting of a 'hard' ceramic strike face and a 'soft' metal or composite backing are used for ballistic protection in both vehicles and body armour. The role of the ceramic is to erode and blunt the hard tip of the projectile, while the role of the backing material is to absorb the residual energy of the eroded projectile and fragments of the cracked ceramic [1-4]. One of the advantages of employing ceramic/composite hybrid armour, compared to materials such as steel and aluminium, is that more lightweight systems can be designed. The load on vehicle or soldier is reduced and the mobility is thereby improved.

Impact of a projectile on a ceramic strike face will result in fragmentation and cracking of the ceramic tile, since the ceramic dissipate kinetic energy from the projectile by fracture [5]. Furthermore, tensile stresses will appear on the back of the tile, i.e. at the interface between the ceramic and the backing material that is bonded to it. The extent of the tensile stresses depends primarily on the intensity of the impact shock wave that reaches the back face, and on the reflection of the stress waves back into the ceramic. A big difference in mechanical impedance between the two bonded materials will result in a low transmission of energy. Most of the incident energy will then be reflected back into the ceramic, thus increasing the tensile stresses and the cracking of the tile. It is therefore desirable that the two bonded materials have impedances that are relatively similar or, when an adhesive is applied, that the impedance of the adhesive is similar to the impedance of the ceramic (and preferably also that of the backing material) [1]. Although this may be difficult to achieve in practical terms, it is nevertheless believed that one aspect of armour systems that could increase the ballistic performance, is the tuning of the interface between the materials that are bonded together [6].

The effect of the adhesive and the adhesive bondline in armour systems has also been investigated by modelling [3, 7]. Zaera et al. [7] concluded that a thicker layer of the adhesive in a ceramic/metal armour system results in a higher area of plastic deformation of the metal backing plate, giving higher absorption of the kinetic energy

DOI til publisert versjon / DOI to published version: 10.1016/j.ijadhadh.2015.07.015

of the projectile. On the other hand, in order to reduce the fragmentation of the ceramic tile, the thickness of the adhesive layer should be reduced as much as possible since this is expected to increase the erosion of the projectile. These are two opposing effects. The fragmentation of the ceramic material, which will reduce the erosion of the projectile is, however, expected to be of greater importance. The effect of the interfacial adhesion between materials was not discussed in refs. [3, 7].

The effect of the interfacial bond in armour systems have been investigated by several authors. This includes surface treatment of some of the most common ceramic materials, such as alumina, boron carbide and silicon carbide [5]. The main purpose of the surface treatment is to remove weak boundary layers (e.g. oils and greases) from the surface, maximise the degree of molecular contact between the surface and the adhesive, and to ensure that the intrinsic adhesion forces across the interface are sufficient to achieve adequate bond strength [8]. Methods to prepare ceramic surfaces for adhesive bonding include grit-blasting [9-11], abrasion [12], plasma [13-15], laser ablation [9, 16], sol-gel [10, 11] and silane treatment [17-19]. In some of these studies, the main focus was on the evaluation of the effect of the adhesive bondline between ceramic tiles and a metal backing plate. Nevertheless, in all the listed studies it was found that the adhesive strength to the ceramic could be improved by surface treatments when an adhesive was employed to bond the materials together. As a special application, bonding to dental ceramic materials is also a much discussed topic [20].

Although the adhesion between different materials has been investigated, little work has been published on the subsequent effect on the ballistic performance of armour systems. One exception is the work conducted by Harris et al. [9, 16]. They found that the adhesive bond strength to both alumina and silicon carbide could be improved when employing epoxy adhesives. They suggested that this was due to an increased concentration of hydroxyl groups on the ceramic surfaces as the result of a laser treatment. An increase in hydroxyl group concentration will provide for better chemical interaction with the epoxy adhesive, thus improving the bond strength. Harris et al. also conducted ballistic testing on panels that were made from ceramic tiles backed by adhesively bonded sheets made from a ballistic fibre [21]. The testing suggested that improved ceramic/adhesive bond strength had an effect on the ballistic

performance of the panels, e.g. by giving less delamination between the ceramic and the backing. This could also explain the improved resistance to multi-hit that was observed upon multiple projectile impacts.

A number of different quasi-static test methods have been used to evaluate the adhesion to ceramic materials, including butt joint, double lap shear, shear by compression loading, asymmetric wedge, flexural and peel tests [9-12, 15-17, 19, 22, 23]. However, one common challenge for many of these tests is that the fabrication of test specimens can be quite complicated, and also that one particular test may be required for one particular type of bonded joint. In cases where at least one of the adherends is relatively flexible, the peel test may therefore be an attractive alternative. The test specimen in a peel test can usually be prepared by bonding, or fusing, the two adherend sheets together, making the specimen preparation quite simple. There are a number of different types of peel tests for measurement of adhesion. However, the basic principle is relatively similar for the different peel tests, in that the average peel force per unit width of a rectangular specimen, i.e. the peel strength, is determined [24]. For adhesion testing of a relatively flexible adherend, such as a fibre-reinforced composite material, and a rigid substrate, such as a ceramic material, different variants of peel tests have been employed [25-27]. For flexible-to-rigid assemblies, where the flexible adherend is a fibre-composite, one alternative is the fixed arm peel test [28]. Here, the peel angle is maintained constant by allowing the rigid substrate, which is attached to a jig, to move along a linear bearing system during the test.

In the present work, the effect of surface treatment of an alumina ceramic on the adhesion to a glass fibre-reinforced polymer composite has been investigated. The composite matrix was thermoplastic polyester. Alumina tiles that are representative of alumina used in light-weight body armour were subjected to different surface treatments. The resulting alumina surfaces were investigated by scanning electron microscopy, profilometry, contact angle measurements and X-ray photoelectron spectroscopy, meaning that both topographic and chemical information about the state of the surface was obtained. Test specimens of the alumina and the composite were prepared by a vacuum moulding technique, in which the use of adhesive was not necessary to obtain good adhesion between the two materials. The alumina/composite adhesion was thereafter investigated by the means of the fixed arm peel test. The

ballistic effect of the adhesion is not discussed in this paper, but is currently being investigated.

2 Experimental

2.1 Materials

The alumina (aluminium oxide, Al_2O_3) investigated was Alotec 98 SB from CeramTec (Plochingen, Germany). The alumina content of the ceramic was 98%, with density 3.8 g/cm^3, porosity < 2%, medium grain size 6 µm, Vickers hardness 13.5 GPa, and Young‘s modulus 335 GPa. The size of the alumina ceramic tiles was 150 mm × 150 mm × 10 mm.

The composite that was used was glass fibre in a thermoplastic polyester (low-melting-temperature polyethylene terephthalate, LPET) matrix, delivered by Comfil (Gjern, Denmark). The LPET polymer has been shown to form a consolidated matrix with low porosity content in vacuum-assisted moulding processes [29]. A woven fabric of glass fibre and LPET (balanced twill 2/2) was employed. Composite yarns were first produced by blending glass fibres and thermoplastic fibres in a commingling process. For the consolidated composite material, the fibre content was 57% by weight and 42% by volume, and the density was 1.87 g/cm^3.

The γ-glycidyloxypropyltrimethoxysilane (GPS) coupling agent, used for surface treatment of the alumina, was supplied by Sigma Aldrich. GPS is a commonly used coupling agent, but it was not expected to form covalent bonds with the thermoplastic polyester. However, some degree of mutual solubility, causing interdiffusion of molecular chains, and thereby increasing the interaction between the two phases, was expected.

2.2 Surface treatments

Several surface treatments were applied to the alumina ceramic for improved adhesion to the glass fibre/polyester composite, as summarised in Table 1. In addition to the surface treatments, the as-received alumina was also subjected to surface analysis and peel testing for determination of adhesion strength.

Dette er en postprint-versjon / This is a postprint version.
DOI til publisert versjon / DOI to published version: 10.1016/j.ijadhadh.2015.07.015

Table 1 Surface treatment procedures.

Surface treatment	**Procedure**
As-received	n/a
Degreased	acetone degrease
FPL etched	acetone degrease; etching in two parts sodium dichromate, ten parts sulphuric acid and 30 parts water; 10 min at 55-60°C
Plasma treated	acetone degrease; plasma treatment in Ar; 100 sec at gas flow 10 sccm, pressure 20-25 Pa, RF generator power 100 W and frequency 13.56 MHz
Grit-blasted	acetone degrease; grit-blasting with aluminium oxide grit ≤ 1 mm; acetone wash
Silane treated	acetone degrease; silane treatment in 1 wt.% GPS; one hour hydrolysis in pH 5 water; 10 min immersion; 60 min drying at 93°C

The investigated surface treatments were:

- *Acetone degrease*: The alumina was immersed in acetone for at least 15 minutes, thoroughly rinsed with acetone, and then allowed to dry at room temperature. The acetone degrease was also applied to the alumina prior to the other surface treatments.
- *FPL etch*: The alumina was etched in a chromic-sulphuric acid solution made of two parts sodium dichromate, ten parts sulphuric acid, and 30 parts water by weight [30]. The solution was kept at 55-60°C, and the tiles were immersed for 10 min, rinsed in distilled water, air dried for 10 min, and finally dried at 60°C for another 10 min. The FPL etch is frequently used on aluminium in the aerospace industry and was included as a benchmark reference.
- *Plasma treatment*: The plasma treatment was conducted in a mixture of air and argon (Ar) in a Piccolo plasma chamber from Plasma Electronic. The treatment was conducted at a chamber pressure of 20-25 Pa, an Ar gas flow of 10 sccm, an RF generator power of 100 W, and a frequency of 13.56 MHz. The ceramic tiles were plasma treated for 100 sec.

DOI til publisert versjon / DOI to published version: 10.1016/j.ijadhadh.2015.07.015

– *Grit-blasting*: Grit-blasting was conducted using iron-free aluminium oxide grit with varying shape and grain size up to 1 mm (K 040, Trond T. Wikant, Norway). The chemical composition of the grains also varied. After the grit-blasting, the alumina tiles were washed in acetone.
– *Silane treatment*: Silanisation of the alumina was performed in a 1 wt.% solution of GPS in distilled water [31, 32]. The pH of the solution was adjusted to 5.0 using acetic acid, and the solution was then continuously stirred for 60 min at ambient temperature, using a magnetic stirrer, for hydrolysis of the silane methoxy groups, see Figure 1. The silane was then deposited on the ceramic tiles by immersing them in the solution for 10 min; after which they were dried at 93^{o}C for 60 min.

(a)

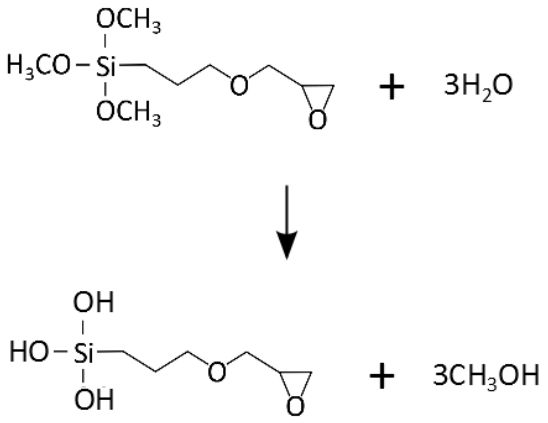

(b)

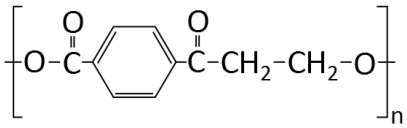

Figure 1 (a) Hydrolysis reaction of the GPS silane. (b) Chemical structure of polyethylene terephthalate (PET).

2.3 Microscopy

Scanning electron microscopy (SEM) was performed on a Hitachi SU6600 Schottky Field Emission Analytical SEM. In some cases, the samples were coated with a 10 nm thick layer of a Pt/Pd alloy prior to imaging. The acceleration voltage was between 1

kV and 10 kV, with the higher acceleration voltage employed for the coated samples. The secondary electrons detector was employed to obtain the images.

Light microscopy was performed on a Carl Zeiss Axio Imager M1m microscope. The investigated samples were first polished employing a selection of diamond particle dispersions to obtain an even surface without scratches.

2.4 Surface topography

For measurement of surface topography, a SENSOFAR PLμ 2300 non-contact, light profilometer from Schaefer Tec was used. The sample was scanned at three different locations. Each scan consisted of 201 planes in the z-direction, with a step length of 0.1 μm between the planes. Three different surface parameters are reported here [33], that is, S_{dr}, S_a, and S_q. The parameter S_{dr} is the relative increase (in %) in surface area of a rough surface, compared to a completely planar surface. S_{dr} is defined as

$$S_{dr} = \frac{A_{rough} - A_{flat}}{A_{flat}} \cdot 100\% \tag{1}$$

where A_{rough} is the surface area of a surface with roughness, while A_{flat} is the surface area of a completely planar surface. The average height deviation of the surface, S_a, is defined as

$$S_a = \frac{1}{MN} \sum_{j=1}^{N} \sum_{i=1}^{M} \left| \eta\left(x_i, y_j\right) \right| \tag{2}$$

where M and N are the number of points in y- and x-direction, respectively, and η is the height of each point relative to a fixed plane. The root-mean-square height deviation of the surface, S_q, is defined as

$$S_q = \sqrt{\frac{1}{MN} \sum_{j=1}^{N} \sum_{i=1}^{M} \eta^2\left(x_i, y_j\right)} \tag{3}$$

Dette er en postprint-versjon / This is a postprint version.
DOI til publisert versjon / DOI to published version: 10.1016/j.ijadhadh.2015.07.015

The use of the letter S indicates that the entire three-dimensional surface was used to calculate the surface parameters [33].

2.5 Compositional analysis

X-ray photoelectron spectroscopy (XPS) was conducted using an AXIS Ultra DLD spectrometer from Kratos Analytical. A monochromatic Al Kα anode with hν = 1486.69 eV was employed. The emission was set to 10 mA, and the pass energy was set to 160 eV with a step size of 1eV for the survey scans, and 20 eV with a step size of 0.1 eV for the high resolution scans. Charge neutralisation was applied since the samples are poor conductors. The XPS spectra were analysed by means of the CasaXPS program (Casa Software Ltd.).

2.6 Contact angle measurements

Contact angle measurements were conducted for water and diiodomethane by a contact angle goniometer equipped with an automatic dispenser (ramé-hart instruments co., Model 200). The advancing contact angle was measured by placing a 5 µL drop of the liquid on the surface, and then increasing the drop volume in steps of 5 µL. Measurements were made after each step. Measurements were also made at multiple locations on the surface. A sufficient number of measurements were made in order to bring the standard deviation of the average value below 1 mJ/m^2. The dispersive and polar components of the surface free energy were calculated by the supplied (DROPimage® Standard) program by means of the two-liquid method. This uses the 'extended Fowkes theory' by assuming the geometric mean for both the polar and dispersive parts of the work of adhesion, i.e.

$$W_{12}^a = \gamma_1(1+\cos\theta) = 2\left(\gamma_1^d\gamma_2^d\right)^{1/2} + 2\left(\gamma_1^p\gamma_2^p\right)^{1/2} \quad (4)$$

where θ is the contact angle, γ_1 and γ_2 are the surface free energies of the liquid and solid, respectively, and the superscripts d and p denotes the dispersive and polar components of the surface free energy.

2.7 Test specimen preparation

Rectangular ceramic/composite specimens were prepared for peel testing. First, five layers of the woven glass fibre/polyester fabric were placed on the surface treated alumina tile. The fabric was extended beyond the edge of the alumina tile, as illustrated in Figure 2(a), to form the material for a peel arm. Along the same edge, a fluoropolymer film was placed between the ceramic and the fabric, extending 20 mm from the edge. The film was placed there to act as a starter crack during the peel testing. Thus, the specimen length available for testing was around 130 mm. Second, the ceramic/fabric was heated to 215°C for 75 min under vacuum. A custom-made vacuum oven, where the bottom part consisted of a heated aluminium plate and the top part consisted of a silicon bag attached to a metal frame, was employed. The silicon bag provided an air tight sealing, and thus allowed for the formation of vacuum inside the 'chamber'. The high temperature resulted in melting of the thermoplastic polyester fibres, and subsequent consolidation of the composite matrix upon cooling. Third, after cooling the panel of the ceramic tile and the consolidated composite material where cut into five peel test samples of width 20 mm, see Figure 2(b). An illustration of the peel test specimen, with the dimensions indicated, is shown in Figure 2(c). As a result of the production process (no adhesive was applied), the polyester matrix provided the adhesion between the alumina and the composite. Thus, there was direct contact between the alumina and the polyester, as illustrated in the ceramic/composite cross-sections shown in Figure 3.

The thickness of the consolidated composite was 1.9 ± 0.1 mm, which was found to be satisfactory for the peel testing. Peel tests employing a thinner composite peel arm resulted in composite fracture close to the crack tip due to bending. The somewhat high variation in composite thickness was a result of the relatively low fibre volume and the flow of the molten polyester during the vacuum-assisted production. It should be pointed out, however, that fibre content (i.e. number of fibres) was the same independent of peel arm thickness.

2.8 Peel testing

The fixed arm peel test was used to evaluate the adhesion between the surface treated alumina and the consolidated composite material [28]. The testing was performed using a Zwick BZ 2.5/TN1S testing machine together with a custom-built test fixture.

The test fixture consisted of an angled specimen holder attached to a table on a linear bearing system. The peel angle was set to 45°. (The actual angle at the crack tip was obviously much lower than 45^{o}.) Higher angles could not be used as this resulted in breaking of the composite arm during testing. To prevent slipping, the specimen was attached very firmly to the holder by a clamping mechanism. This experimental set-up allowed the specimen to slide sideways when the composite peel arm was gripped and a pulling force was applied, see Figure 4.

(a) (b)

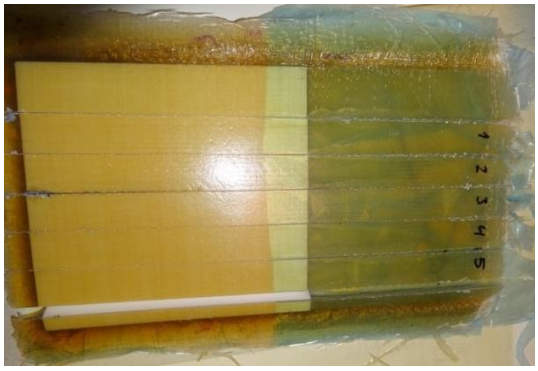

(c)

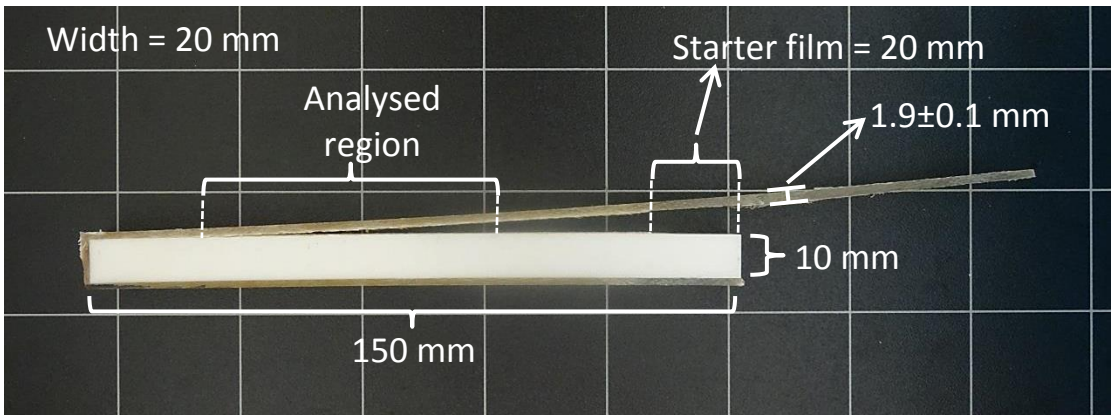

Figure 2 Peel test specimen fabrication: (a) Lay-up of alumina, fluoropolymer film and alumina tile, and (b) five numbered specimens cut from consolidated alumina/composite panel. (c) Illustration of a tested peel test specimen with the dimensions indicated.

DOI til publisert versjon / DOI to published version: 10.1016/j.ijadhadh.2015.07.015

(a) (b)

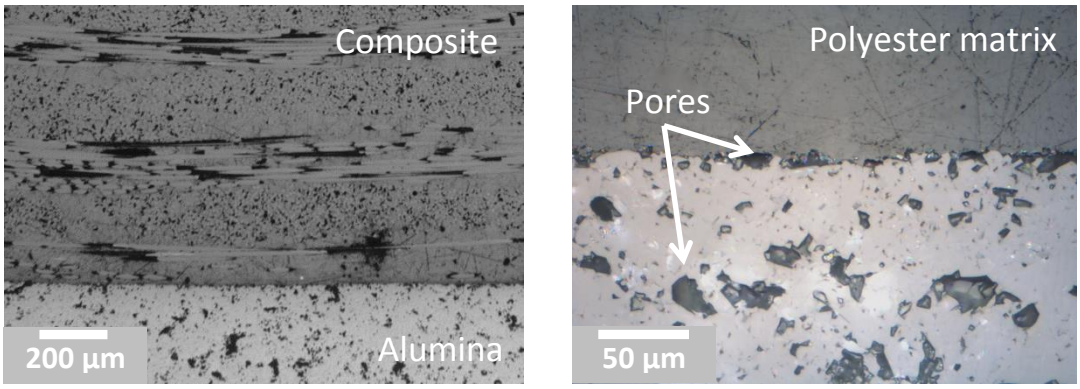

Figure 3 Microscopy images of a cross-section of the consolidated glass fibre/polyester composite bonded to the as-received alumina substrate. (a) Composite with fibre lay-up visible in contact with alumina. (b) Close-up of the alumina/polyester matrix interface from an area with no glass fibres.

The crosshead speed of the test machine was set to 2.93 mm/min, which resulted in an average crack growth rate of the propagating crack of 10.0 mm/min [28]. During the testing, a force versus displacement curve was recorded, and this curve was then used to evaluate the peel strength of the specimen. The force was set to zero prior to gripping the peel arm.

Around 120 mm of peel fracture could usually be established for each alumina surface. In the region close to the starter film, however, abnormalities in the form of irregular high loads were observed prior to the establishment of a propagating crack. The data from this region, as well as data from the end of the specimen, were therefore not included in the calculation of the average peel strength. Thus, the region between a crosshead displacement of 10 mm and 30 mm was taken into account, which corresponded to around 70 mm of peel fracture in the 45^{o} set-up. (For the silane treated alumina, the length of the peel fracture in this region was varying from 62 mm to 70 mm. This can be attributed to the 'stick-slip' behaviour described in Section 3.2.) The peel strength was obtained by dividing the average force in the analysed region with the average specimen width in the same region. A minimum of five specimens for each surface treatment were tested.

(a) (b)

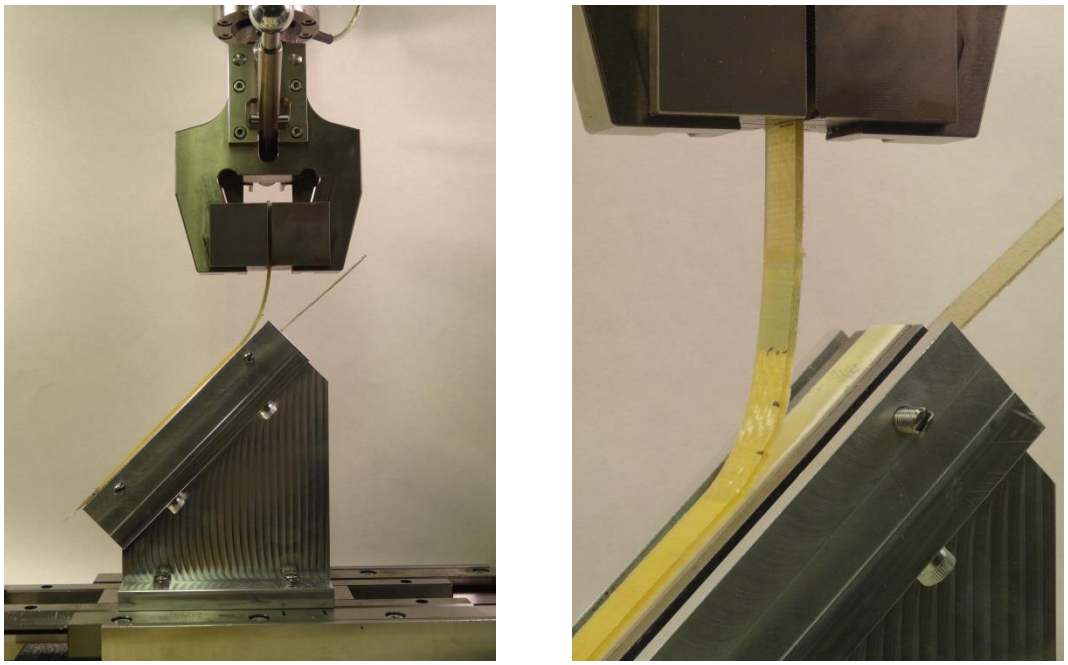

Figure 4 Fixed arm peel test at 45°. (a) Before the test, and (b) detail from the initial test phase.

3 Results and discussion

3.1 Surface analysis of alumina

3.1.1 Scanning electron microscopy

SEM images of the alumina surfaces are shown in Figure 5. The ceramic grains of the as-received surface are clearly visible, as well as grooves between the grains. The degreased, FPL etched and plasma treated surfaces are not shown here since the appearance is similar to the as-received surface. However, the grains are not visible on the grit-blasted surface, which seems to have been eroded by the aluminium oxide grit. On the silane treated surface, a cross-linked silane layer that was formed when depositing and drying the hydrolysed silane is clearly visible. The thickness of this layer, however, seems to vary on the alumina surface. In some areas, the layer is thick enough to completely cover the grooves between the ceramic grains, and only the top of the grains are visible, see Figure 5(c). Pores in the surface have also been filled and are covered by the silane. In other areas, the silane layer is much thinner, and the grains are still clearly visible, see Figure 5(d). A silane layer nevertheless seems to be

present on the surface also here. This variation in layer thickness on the surface was also observed visually.

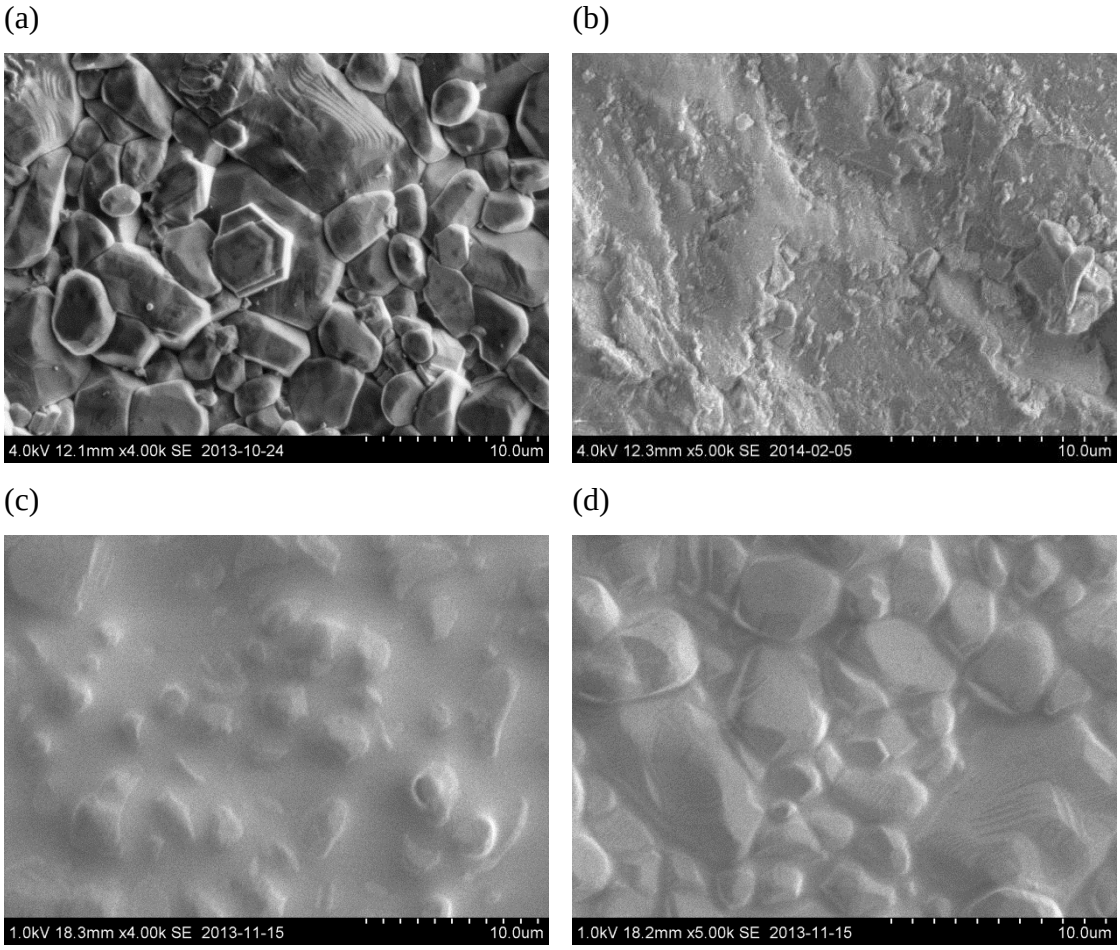

Figure 5 SEM images of alumina surfaces. (a) As-received, (b) grit-blasted, and (c)'thick' and (d) 'thin' silane layer on silane treated alumina.

3.1.2 Profilometry

The surface roughness measurements of the surface treated alumina showed that the surface area parameter, S_{dr}, was relatively similar for most surfaces. The data are given in Table 2. Surface treatments that do not significantly alter the topography of the surface are not expected to change the surface area. For example, the acetone degreased surface does nothing but remove a thin layer of contaminants on the surface, and the value of S_{dr} should therefore be similar to the 64.5% for the as-received alumina. This was indeed the case. However, the surface area of the grit-blasted and the silane treated surfaces deviated from the other alumina surfaces. The

grit-blasted surface gave a higher surface area, with a value for S_{dr} of 127.7%, as well as higher values for S_a and S_q. The silane treated alumina, on the other hand, gave a lower surface area with a value of S_{dr} of 36.6%. This can be explained by the presence of the cross-linked silane layer. The high standard deviance for the surface area, see Table 2, can be explained by the different coverage of the silane layer, giving different thicknesses in different areas of the surface, as shown in the SEM images in Figure 5.

Table 2 Results from profilometry of surface treated alumina.

Surface treatment	**Surface parameter**		
	S_a (µm)	S_q (µm)	S_{dr} (%)
As-received	0.87 ± 0.33	1.11 ± 0.40	64.5 ± 8.8
Degreased	0.73 ± 0.18	0.95 ± 0.23	61.0 ± 7.4
FPL etched	0.73 ± 0.22	0.93 ± 0.27	82.7 ± 19.6
Plasma treated	0.70 ± 0.19	0.90 ± 0.23	76.7 ± 4.4
Grit-blasted	1.44 ± 0.15	1.82 ± 0.16	127.7 ± 4.7
Silane treated	0.64 ± 0.18	0.84 ± 0.31	36.6 ± 21.3

3.1.3 X-ray photoelectron spectroscopy

The elemental composition of the surface treated alumina is given in Table 3. When the as-received alumina surface is acetone degreased, the content of carbon is decreased from 28.7% to 14.1%. This shows that the acetone degrease is relatively efficient in removing contaminants from the alumina surface. It seems that the additional FPL etch is even more efficient in cleaning the alumina, as the Al/C ratio is increased from 1.9 to 2.4, compared to the degreased alumina. After the silane treatment, the carbon content is significantly increased to 35.7%. (The silane treatment was conducted on a previously degreased alumina surface.) The increase is the result of the silane layer being present on the surface, leading to coverage of most of the underlying alumina. The Al/O ratio is relatively similar at 0.5 for most surface treatments. The lower Al/O ratio of the alumina surface, compared to what would be expected from bulk alumina, is due to the presence of aluminium hydroxides in the outer surface layer. This elevates the measured O concentration. For the grit-blasting and silane treatments, the Al/O ratio is reduced to 0.4. For the silane treated surface, this can be explained by the additional contribution from the oxygen that is present in the GPS molecule. Hence, relatively more oxygen is present on the surface, firmly

attached in the form of the cross-linked silane layer. The reason for the decreased value for the grit-blasted surface is believed to be contamination from the aluminium oxide grit used in the grit-blasting.

Table 3 XPS results for surface treated alumina.

Surface treatment	**Elemental concentration (at.%)**								
	Al	O	C	Si	Ca	F	S	Cr	Others
As-received	22.3	43.6	28.7	3.9	1.0	-	-	-	0.6
Degreased	26.9	53.5	14.1	2.8	1.0	-	-	-	1.6
FPL etched	26.9	55.9	11.1	1.6	0.5	-	1.3	2.9	-
Plasma treated	25.6	52.0	14.0	2.3	2.0	3.6	-	-	0.4
Grit-blasted	22.4	55.6	15.2	3.3	1.2	0.3	-	-	2.0
Silane treated	16.7	43.0	35.7	4.4	0.3	-	-	-	-

3.1.4 Contact angle measurements

The contact angle measurements are an important complement to the surface roughness and XPS data because the surface free energy of a material is very important for the wetting and adhesion properties of the surface. Contact angles are also quite sensitive to changes in the topmost molecules of the surface. The results from the contact angle measurements are given in Table 4. The calculated surface free energy of all alumina surfaces measured here was far lower than the theoretical surface free energy of quasi-amorphous Al_2O_3. The latter is given as 1520 mJ/m^2 for γ-alumina and 1760 mJ/m^2 for α-alumina [34]. The structure of the present surfaces is also quite complex, as observed in the SEM images in Figure 5, consisting of crystals of a few micrometres size and with clearly visible crystal planes. Measured surface free energies for alumina can be quite varying, depending on the type of alumina, crystal structure and orientation, and the polar (acid-base) component as measured by water can also vary with the pH [35]. However, values quite similar to our results have also been found by others [9], so these are as expected for commercial alumina tiles. The large deviation from the theoretical value(s) is usually explained by organic contamination, which may be present even in clean rooms and is difficult to remove completely [36]. The XPS results also show a considerable amount of carbon and other ‘foreign’ molecules on the surface. As can be seen from Table 4, the total surface free energy is always increased as a result of the different surface treatments.

DOI til publisert versjon / DOI to published version: 10.1016/j.ijadhadh.2015.07.015

This is a good indication that carbon-based contaminants were present on the as-received alumina surface, and that these contaminants are to some extent removed by, e.g., the degreasing step in acetone. It is interesting to note that the increase in total surface free energy is mostly the result of an increase in the dispersive component of the surface free energy, while the polar component does not change very much as a result of the cleaning procedures. However, the grit-blasting and silane treatments result in a decrease of the polar component. For the silane treated surface, this is obviously the result of the deposition of additional organic molecules on the surface.

Table 4 Contact angles and surface free energies of surface treated alumina.

Surface treatment	**Contact angle (^{o})**		**Surface free energy (mJ/m^2)**		
	Water	Diiodomethane	Polar	Dispersive	Total
As-received	45.4 ± 1.0	70.4 ± 0.6	31.0	22.6	53.6
Degreased	32.6 ± 0.3	48.9 ± 0.4	30.6	34.9	65.5
FPL etched	25.6 ± 0.5	37.5 ± 0.6	30.4	40.8	71.3
Plasma treated	16.7 ± 0.5	34.8 ± 0.4	32.9	42.1	75.0
Grit-blasted	40.3 ± 0.7	30.3 ± 0.4	21.6	44.1	65.7
Silane treated	39.6 ± 0.4	25.6 ± 0.6	21.1	45.9	67.0

With the reservation that the two-liquid method for surface free energy is a debated, although much used, method there are some explanations that may be attempted, especially when seen together with the XPS results. The cleaning steps result in less organic contaminants on the surface, but do not remove these completely. It has been proposed that the polar component of the surface free energy is more sensitive to very small amounts of contamination than the dispersive component. This is because of the longer range of the dispersive van der Waals forces than the polar forces [37], as the latter are only operating in the topmost atomic layer. If even only one (strongly adsorbed) monomolecular layer of contaminant is left, the polar forces are mostly due to the structure of that layer, while the dispersive forces increase with a decreased layer thickness because of the undelaying aluminium. XPS also probes a depth of a few nm, which is more than a monomolecular layer thickness. In addition, the roughness of the alumina surface must be taken into consideration, as the layer thickness is probably not uniform. The increased dispersive component for the silane treated surface is, however, not easily explained by this argumentation. The amount of silicon in the surface is higher than the other samples, and this must be due to the

silane groups in this relatively thick layer (as seen from the SEM pictures in Figure 5), but this increase is not very high compared to the as-received sample and cannot alone explain the increased dispersive component. The contact angles, and thus the surface free energies, may be corrected for the surface roughness by using Wenzel's equation,

$$\cos\theta^* = r\cos\theta \tag{5}$$

where θ^* is the apparent (measured) contact angle and is θ the 'true' angle. The ratio r is the roughness ratio which is defined as the ratio of the true area of the solid surface to the apparent area. This ratio can be calculated from S_{dr} from the profilometer measurements and will lead to higher angles and lower calculated surface free energies. However, given the inaccuracy of the profilometer measurements, we judge this will not give a considerable improvement of this discussion and we have therefore chosen not to do this. The calculated high dispersive component of the surface free energy is mainly a result of a lowered contact angle of diiodomethane, and one should be aware of the possibility of this liquid partly dissolving some of the surface layer. This will result in an artificially high dispersive component. Given these uncertainties, we have chosen not to discuss the contact angle results in more detail.

3.2 Peel test results

All the different surface treatments resulted in an increase in peel strength from the initial value of 9.6 N/mm of the as-received surface, see Table 5. The peel strength after the acetone degrease and the FPL etch were 13.8 N/mm and 15.7 N/mm, respectively, while the highest value was recorded for the silane treated alumina with a peel strength of 19.9 N/mm. Thus, there was an increase of 100% relative to the as-received alumina.

In cases with relatively poor adhesion, such as for the as-received alumina, the crack was usually propagating in a stable manner. However, as the alumina/polyester adhesion was increased, a higher tendency of unstable crack growth was observed. This 'stick-slip' behaviour [38] is illustrated in Figure 6, where examples of peel curves are shown. In some sections along the length of the peel specimen, the crack then propagates at much higher velocity than during the stable crack growth, thus releasing the high loads that have been building up.

In Figure 6(a), the stable crack growth of the as-received alumina can be seen. The stable crack growth makes it relatively straightforward to calculate an average value of the peel force. As the alumina/polyester adhesion is increased, more unstable crack growth is observed. This is clearly illustrated in Figure 6(b) and Figure 6(c) for the acetone degreased and silane treated alumina, respectively. An average value of the peel force could be calculated also in these cases. However, the difference between the highest and lowest measured force is of a different magnitude when the unstable crack growth behaviour occurs.

In the type of joints that were tested here, there are several possibilities for the locus of failure of the propagating crack. These include: (1) interfacial failure between the alumina ceramic and the polyester matrix of the composite, (2) cohesive failure in the polyester matrix, (3) interfacial failure between the glass fibres and the polyester matrix, and (4) inter- or intralaminar failure in the composite, including fibre breakage. In most cases, combinations of these failure modes, such as e.g. simultaneous matrix failure and fibre/matrix failure, will probably occur. Therefore, to determine what the failure mode was in the tested joints, the fracture surfaces were evaluated visually using a stereo microscope. One advantage of using this technique at a relatively low magnification, is that a larger area can be evaluated compared to other microscopy techniques. Hence, a better overview of the fracture surface of several specimens can be obtained but at the expense of not being able to detect smaller details. For example, a thin layer of polyester on the alumina may be interpreted as alumina/polyester interfacial failure, while the failure may actually be cohesive within the polyester matrix.

As can be seen from Table 5, there is a general trend that the locus of failure apparently shifts from the alumina/polyester interface towards cohesive within the composite material with increasing peel strength. For the as-received alumina, mainly alumina/polyester interfacial failure is observed. However, for the silane treated alumina, which gave the highest peel strength, little of the failure appears to be interfacial. Thus, the growing crack is forced to propagate inside the composite when the adhesion between the alumina and the polyester is increased.

(a)

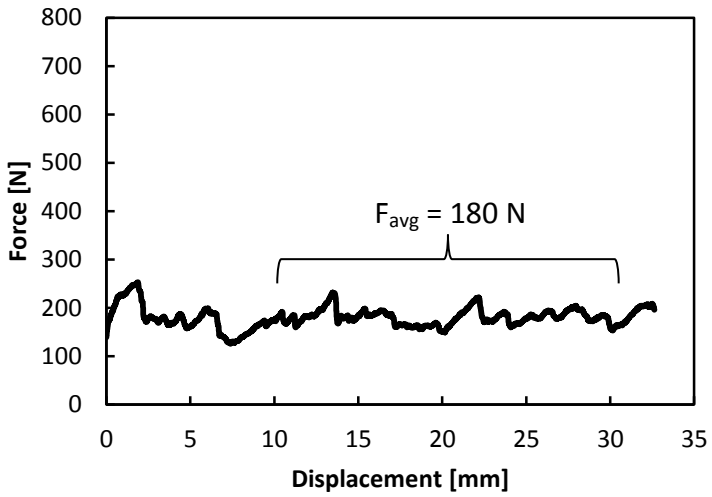

(b)

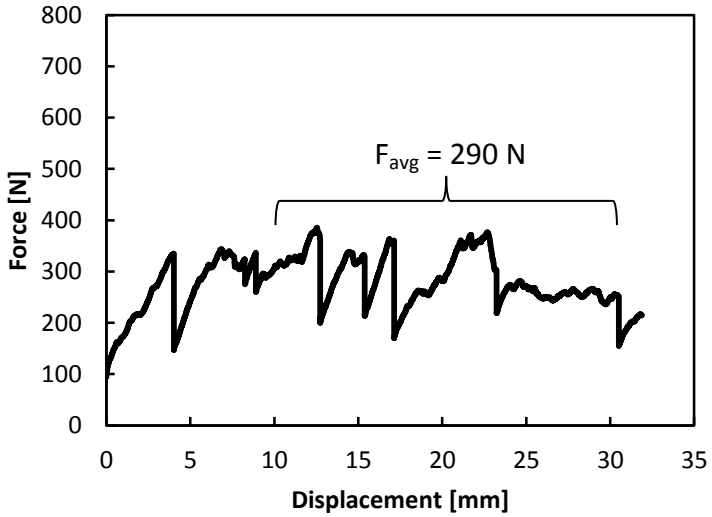

(c)

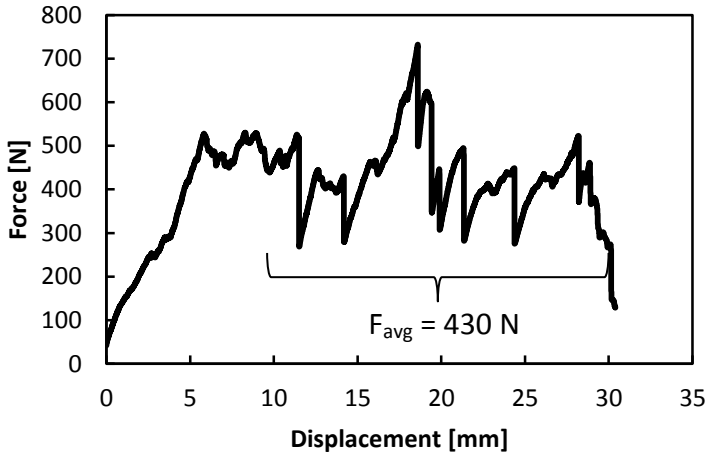

Figure 6 Peel curves for alumina surfaces: (a) as-received, (b) degreased and (c) silane treated.

DOI til publisert versjon / DOI to published version: 10.1016/j.ijadhadh.2015.07.015

Table 5 Peel test results obtained for surface treated alumina.

Surface treatment	**Peel strength (N/mm)**	**Locus of failure by visual observation**
As-received	9.6 ± 0.6	Mainly interfacial, some cohesive[1]
Degreased	13.8 ± 0.9	Mixed interfacial and cohesive
FPL etched	15.7 ± 0.9	Mixed interfacial and cohesive
Plasma treated	12.6 ± 0.6	Mainly cohesive, some interfacial
Grit-blasted	13.2 ± 1.9	Mainly cohesive, some interfacial
Silane treated	19.9 ± 2.3	Cohesive

3.3 Failure surface fractography

To obtain a better understanding of the failure mode, a more detailed investigation of the fracture surfaces was needed. In addition to the visual observations, scanning electron microscopy was therefore used to evaluate the fracture surfaces. In Figure 7, SEM overview images that were prepared by merging several micrographs are shown.

The SEM investigation at relatively low magnifications was able to confirm the visual observations. Interfacial failure is mainly observed for the as-received surface and, as can be seen from Figure 7(a), little of the composite material is attached to the alumina side of the fracture. This seems to change for the substrates that gave higher peel strengths. For example, more composite is left on the degreased and FPL etched substrates, see Figure 7(b-c), and there seems to be a combination of alumina/polyester interfacial failure and failure within the composite material. This behaviour is also seen to a varying extent for all the other substrates, with the exception of the silane treated substrate. On this substrate, which gave the highest peel strength, very little interfacial failure could be observed and the failure was almost exclusively in the composite material, see Figure 7(f).

More detailed SEM images of the fracture surfaces are shown in Figure 8. An example of alumina/polyester interfacial failure on the as-received substrate is shown in Figure 8(a-b). Little of the thermoplastic matrix remains on the ceramic side of the fracture surface, the alumina grains are relatively bare, whereas the imprints of the grains are clearly observed on the opposite composite fracture surface. These two

[1] The term ‘cohesive’ in the table relates to all types of fracture modes where the crack propagates inside the composite material, thus away from the alumina/polyester interface.

observations, which are a sign of a relatively low degree of adhesion between the ceramic and the composite, were typical also for the other surfaces where interfacial failure was seen. Ductile drawing during fracture of the thermoplastic that was attached between the grain boundaries on the ceramic surface is also evident from the SEM images.

On some of the substrates, such as degreased alumina, the higher magnification SEM revealed areas with a thin layer of polyester on the alumina. An example is shown in Figure 8(c), where there is a transition between failure that is clearly in the polyester matrix on the left side of the image, and failure close to the alumina surface on the right side of the image. In the latter case, the failure is also in the polyester matrix, and a thin layer of the matrix is left on the surface. In these areas, the alumina grains are not clearly visible but, as discussed above, the locus of failure may misleadingly be interpreted as interfacial by the visual observations. It should be pointed out that a combination of alumina/polyester interfacial failure, cohesive matrix failure and composite failure was observed on these substrates, and that the failure mode on most of the substrates is relatively complex.

The unstable (‘stick-slip’) fracture behaviour during the peel testing could also be identified in the fracture surfaces. Rapid crack propagation through the polyester matrix produced a relatively smooth surface, while slower crack propagation produced a rougher surface. This is similar to observations described for thermoplastic polymers in the literature, as reported by Greenhalgh [39], with slow fracture typically giving ductile drawing and fibrillation (several examples are shown in Figure 8), while rapid fracture gives a more plane fracture surface with uniformly distributed thermoplastic globules. In fact, small globules less than 100 nm in size were observed in the rapid fracture region in the joints tested here, as shown in Figure 8(d). However, smearing of the thermoplastic matrix may also occur under certain stress states [39]. (This was observed, but is not shown here.)

As expected from the observations discussed above, very little of the failure on the silane treated substrate was interfacial between the alumina and the polyester. Most of the surface was covered with composite material, including glass fibres, and in some places only polyester matrix material. Thus, the specimen failed mainly inside the

composite, with much of the crack propagation taking place in the fibre/matrix interface. This is illustrated in Figure 8(e-f), where examples of fracture surfaces obtained from crack propagation in the composite material are shown. Glass fibres on one fracture surface and imprints of glass fibres on the opposite fracture surface are clearly visible. On the whole, the appearance of the silane treated substrate indicated that the adhesion was higher compared to the other surface treatments, particularly when compared to the as-received alumina substrate. It should be noted, however, that composite failure was to some extent observed in all the tested joints, as illustrated in Figure 7.

3.4 Adhesion mechanisms

There was a good correlation between the measured peel strengths of the different alumina substrates and the failure modes observed by SEM. A relatively low peel strength and mainly alumina/polyester interfacial failure was observed for the as-received substrate. This correlates well with the high carbon content, as measured by XPS, and the relatively low surface free energy, as determined from contact angle measurements, of the surface. Thus, a layer of contamination is probably responsible for lowering the interfacial adhesion.

The FPL etched substrate (that was included as a reference) gave a slightly higher peel strength than the acetone degreased surface. There are also some indications that there was less alumina/polyester interfacial failure after the FPL-etching, although this remains somewhat uncertain and would require a more detailed investigation by SEM. Nevertheless, the FPL etched alumina had a lower carbon content (some traces of sulphur and chromium originating from the etchant were also detected), and a higher surface free energy as the result of the dispersive component of the surface free energy being increased after etching (indicating that the contaminating layer had been partly removed, or become thinner). This indicates that the etching was more efficient in removing the contaminants on the surface, and that better interfacial adhesion was obtained.

(a)

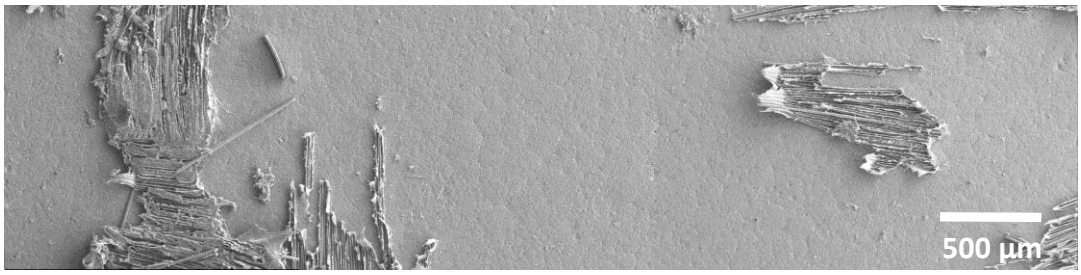

(b)

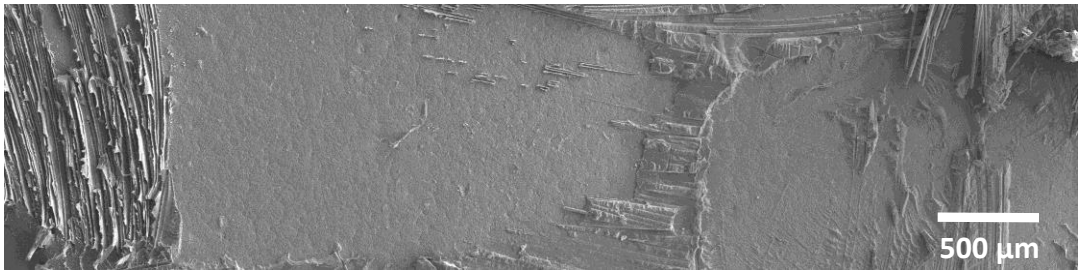

(c)

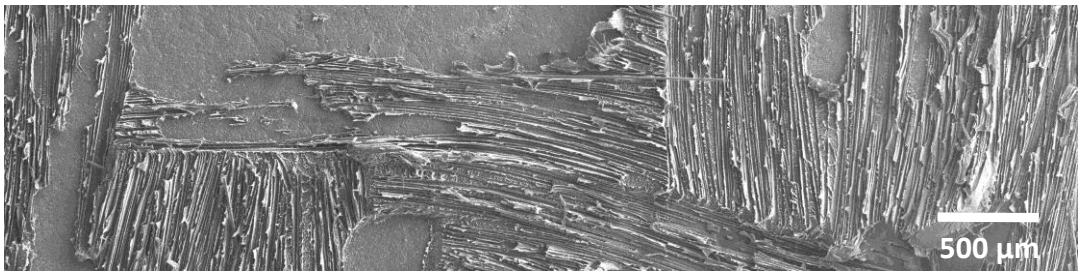

(d)

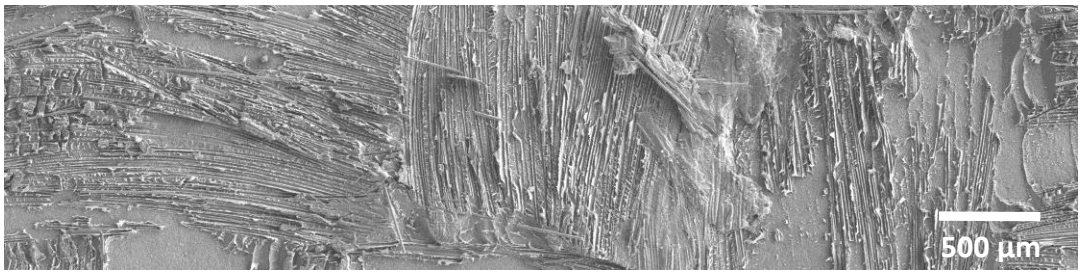

(e)

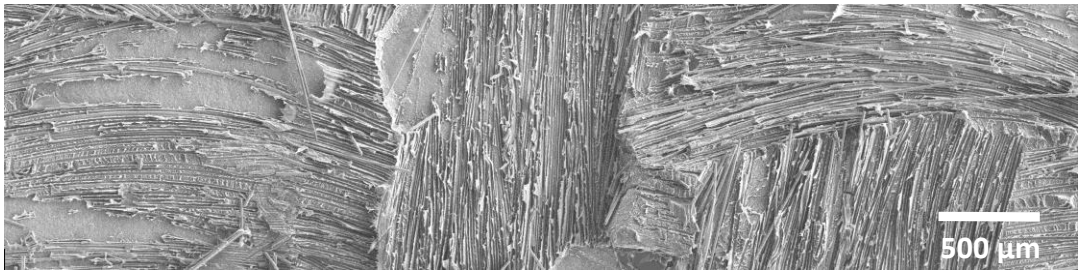

(f)

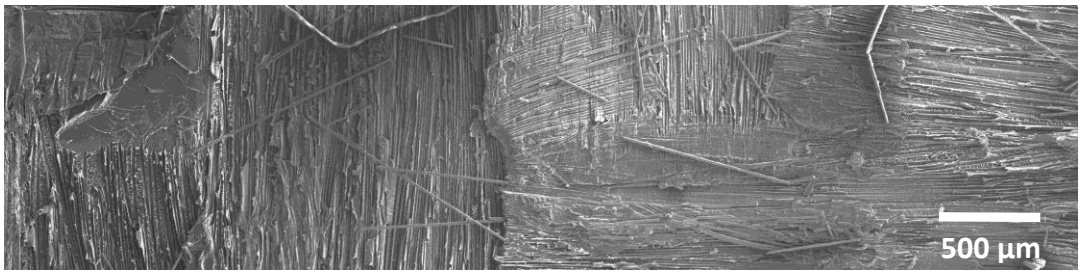

Figure 7 SEM overview images of the alumina side of the fracture surfaces. The overview images were produced by combining several images. (a) As-received, (b) degreased, (c) FPL etched, (d) plasma treated, (e) grit-blasted, and (f) silane treated alumina. The crack growth direction was from left to right.

One effect of improved alumina/polyester interfacial adhesion is that the propagating crack is forced to find another path away from the interface. Once the propagating crack is directed away from the alumina/polyester interface, other energy absorbing fracture mechanisms will occur in the glass fibre composite. These include fibre/matrix interfacial failure and fibre breaking, as was indeed observed by SEM in Figure 8(g). Combinations of fibre/matrix failure and matrix failure close to the fibre surface have also been observed by SEM. However, fracture mechanisms that involve breaking of fibre will absorb significantly more energy compared to matrix, i.e. the ductile drawing of polyester that was observed for alumina/polyester interfacial failure, or fibre/matrix bond failure [40]. The higher strength of the fibres will thus give higher measured peel strengths. Another mechanism that will absorb energy in fibre-composites is localised fibre bridging in the zone behind the crack tip [39, 41, 42]. Here, unbroken fibres connect the two fracture surfaces, forming a ‘bridge’ that may contribute considerably to the higher fracture strength.

The silane treated substrate gave the highest peel strength and the failure was mainly in the composite material. It is well known that the coupling agent GPS has the potential to be an effective adhesion promoter in aluminium/epoxy adhesive joints [31]. The proposed mechanism by which it functions is that the silane that is deposited on the surface acts as a covalent ‘bridge’ between the aluminium oxide, which is always present as a top layer of varying thickness on aluminium surfaces, and the epoxy adhesive. This mechanism has been verified experimentally [32, 43,

44]. GPS has also been used with good result to increase the adhesion between epoxy and ceramics, such as alumina and boron carbide [10, 18]. For the alumina ceramic used here, it is possible that there is a covalent interaction between the surface and the silane. The chemistry of the aluminium surface is quite similar to the alumina, since both are in fact aluminium oxide.

(a)

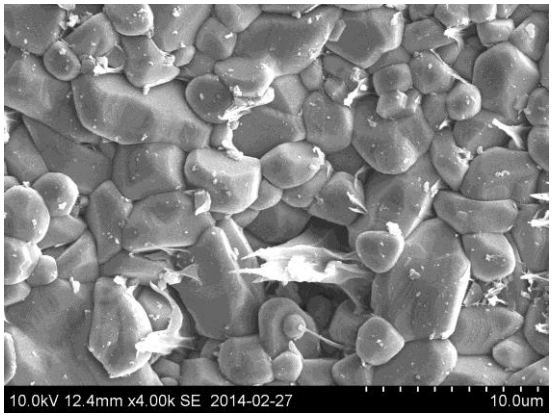

(b)

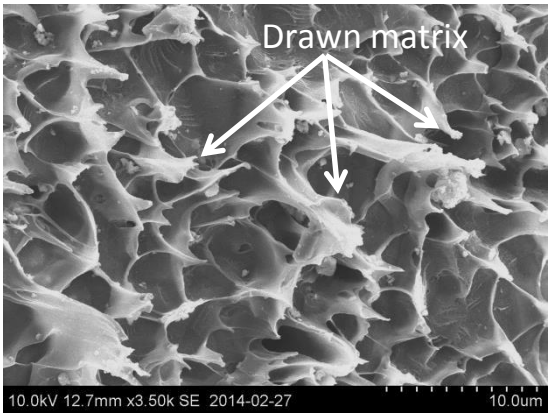

(c)

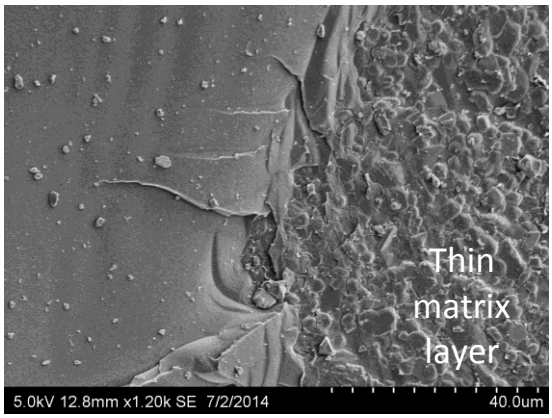

(d)

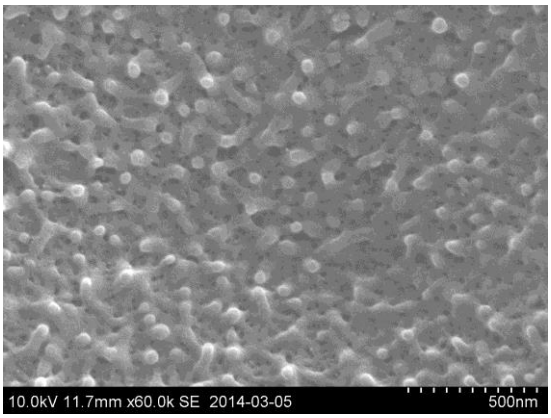

(e)

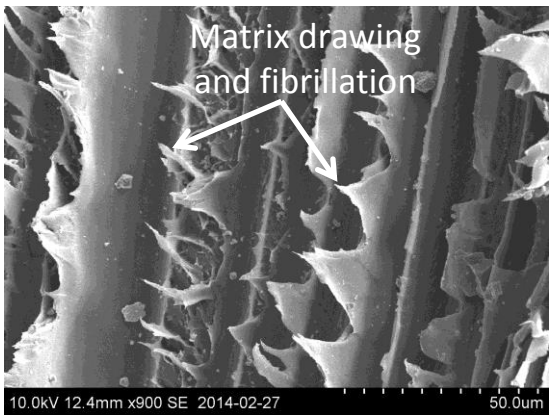

(f)

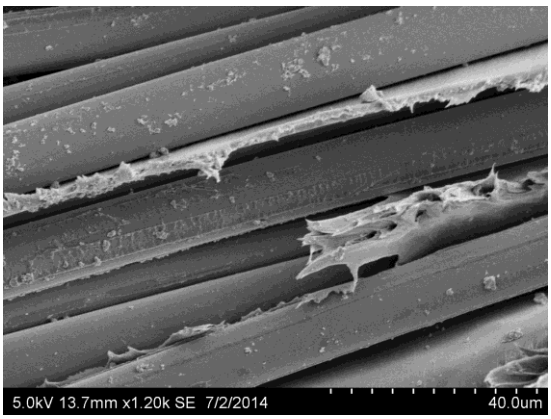

Dette er en postprint-versjon / This is a postprint version.
DOI til publisert versjon / DOI to published version: 10.1016/j.ijadhadh.2015.07.015

(g)

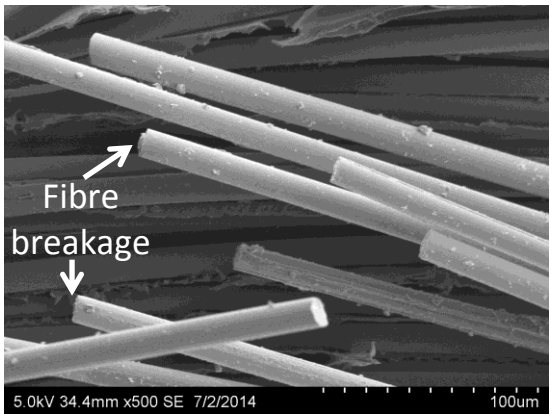

Figure 8 SEM images of fracture surfaces. Alumina/polyester interfacial failure on (a) alumina side and (b) composite side (of as-received substrate). (c) Matrix failure near alumina surface (degreased substrate). (d) Small globules in rapid fracture region of matrix (composite side of silane treated substrate). (e) Fibre/matrix failure, matrix drawing and fibrillation (ceramic side of plasma treated surface). (f) Fibre/matrix failure (composite side of silane treated surface). (g) Fibre breakage (composite side of silane treated surface).

On the other hand, is not obvious that the interaction between the silane and the polyester is of a covalent nature. The chemical structures of the two do not indicate that a reaction forming a covalent bond will take place. Nevertheless, the measured surface free energies may partly explain why the silane treated substrate gave the highest adhesion to the polyester composite. The surface free energy of a polished surface of the neat polyester (no glass fibre) was also measured. The total surface free energy for the polyester was 51.2 mJ/m^2, while the polar and dispersive components were 6.5 mJ/m^2 and 44.7 mJ/m^2, respectively. Thus, a low polar component and a relatively high dispersive component were measured. This result is most comparable to the surface free energies of the silane treated and grit-blasted surfaces in Table 4. The more similar surface free energies of the surface and the polymer indicate that the two organic compounds (silane and polyester) also have similar solubility parameters [45]. This will promote better adhesion between the surfaces as the molecules of the two surfaces may diffuse into each other. This is a well-known mechanism when bonding polymers [46]. Another factor that may play a role is the roughness of the surface. The silane treated surface was relatively flat, with the lowest measured surface area, while the grit-blasted surface had a relatively high roughness, see Table

2. Thus, the more flat silane treated surface may be more easily wetted than the rougher grit-blasted surface if the viscosity of the molten polymer is too high. The polymer may then not be able to penetrate the cracks and crevices on the grit-blasted surface, resulting in an effectively lower interfacial contact area, which may be why the lower peel strength is observed. Van der Waals forces, combined with better wetting of the available surface area, are then possibly the main reasons for the high peel strength of the silane treated surface.

4 Conclusions

The adhesion between an alumina ceramic and a glass fibre-reinforced polyester-matrix composite could be significantly improved after different surface treatments of the alumina. Contact angle measurements and XPS showed that the acetone degreasing removed organic contaminants from the as-received alumina, resulting in higher surface free energies. This effect alone will considerably increase the interfacial adhesion, as was indeed confirmed by the higher peel strength that was measured after cleaning of the alumina surface. Further cleaning was obtained by a subsequent chromic-sulphuric acid etch (FPL etch), resulting in the peel strength being increased even further.

Silane treatment of the alumina with GPS had the greatest effect on the peel strength. There may be several explanations for the increased adhesion that was measured on this substrate. First, covalent bonds are possibly formed between the alumina and the silane, resulting in a strong interaction between the two phases. Second, van der Waals forces are more likely responsible for the interfacial attraction between the silane and the polyester. However, the measured surface free energies indicated that the solubility parameters of the cross-linked silane layer and the polyester are relatively similar, which may give mutual diffusion of the two polymers and thus promoting better adhesion. Third, the silane treated surface had a lower surface area than the other surfaces, but the smoother surface combined with improved wetting will probably reduce the number of defects in the alumina/polyester interface. Poor wetting, on the other hand, such as e.g. on the as-received alumina, will result in areas where there is no direct contact between the alumina and the polyester, thus creating defects in the interface. As a preliminary conclusion, it can be assumed that although

the surface area of the silane treated alumina is lower, the alumina/polyester interphase will be of a higher quality.

The peel strength of the tested joints could be correlated to the appearance of the fracture surfaces. There was a clear trend that the locus of failure shifted from alumina/polyester interfacial failure towards cohesive failure within the composite material when the peel strength was increased. An additional observation was the shift from stable to unstable crack propagation. Thus, an increasing level of adhesion between the alumina and the thermoplastic polyester gave a shift in the crack path of the propagating crack. The higher alumina/polyester adhesion directed the crack to propagate inside the fibre-composite, away from the alumina surface. This will initiate fracture mechanisms that involve the reinforcing glass fibres, which absorb more energy and, hence, higher peel strengths are observed.

Acknowledgements

The authors would like to thank Dr Spyridon Diplas and Grazyna Jonski at the University of Oslo for assistance with the XPS and profilometry measurements. We would also like to thank Dr Luiz F. Kawashita at Cardiff University for valuable discussions about the peel testing.

References

[1] Zaera R. Ballistic impacts on polymer matrix composites, composite armor, personal armor. In: Abrate S, editor. Impact engineering of composite structures, Vienna: Springer; 2011, p. 305-403.

[2] Grujicic M, Pandurangan B, Zecevic U, Koudela KL, Cheeseman BA. Ballistic performance of alumina/S-2 glass-reinforced polymer-matrix composite hybrid lightweight armor against armor piercing (AP) and non-AP projectiles. Multidiscipline Modeling in Materials and Structures 2007;3:287-312.

[3] Grujicic M, Pandurangan B, d'Entremont B. The role of adhesive in the ballistic/structural performance of ceramic/polymer matrix composite hybrid armor. Materials & Design 2012;41:380-393.

[4] Medvedovski E. Ballistic performance of armour ceramics: Influence of design and structure. Part 2. Ceramics International 2010;36:2117-2127.

[5] Medvedovski E. Ballistic performance of armour ceramics: Influence of design and structure. Part 1. Ceramics International 2010;36:2103-2115.

[6] Opportunities in protection materials science and technology for future army applications. Washingon: National Academy of Sciences, The National Academies Press; 2011.

[7] Zaera R, Sanchez-Saez S, Perez-Castellanos JL, Navarro C. Modelling of the adhesive layer in mixed ceramic/metal armours subjected to impact. Composites Part A: Applied Science and Manufacturing 2000;31:823-833.

[8] Kinloch AJ. Adhesion and adhesives: science and technology. London: Chapman and Hall; 1987.

[9] Harris AJ, Vaughan B, Yeomans JA, Smith PA, Burnage ST. Surface preparation of alumina for improved adhesive bond strength in armour applications. Ceramic Engineering and Science Proceedings, Advanced Ceramic Armor VIII 2012;33:149-159.

[10] Bujanda A, Copeland C, Dibelka J, Forster A, Holmes L, Jensen R, Kosik W, McKnight S, Koellhoffer S, Gillespie Jr J. Analysis of adhesively bonded ceramics using an asymmetric wedge test. Aberdeen Proving Ground: U.S. Army Research Laboratory; 2008.

[11] Bujanda A, Forster F, Kosik W, Jensen RE, McKnight SH. Advanced surface treatments and adhesive bonding testing schemes of ceramic assemblies. Aberdeen Proving Ground: U.S. Army Research Laboratory; 2006.

[12] Park R, Jang J. The effect of surface roughness on the adhesion properties of ceramic/hybrid FRP adhesively bonded systems. Journal of Adhesion Science and Technology 1998;12:713-729.

[13] Rodriguez-Santiago V, Vargas-Gonzalez L, Bujanda AA, Baeza JA, Fleischman MS, Yim JH, Pappas DD. Modification of silicon carbide surfaces by atmospheric pressure plasma for composite applications, ACS Applied Materials & Interfaces 2013;5:4725-4730.

[14] Bujanda AA, Rodriguez-Santiago V, Ho CC, Stein CE, Jensen RE, Pappas DD. Atmospheric plasma treatment of polymer films and alumina ceramics for enhanced adhesive bonding. Proc. 34th Annual Meeting of the Adhesion Society. Savannah; 2011.

[15] Asai H, Iwase N, Suga T. Influence of ceramic surface treatment on peel-off strength between aluminum nitride and epoxy-modified polyaminobismaleimide adhesive. IEEE Transactions on Advanced Packaging 2001;24:104-112.

[16] Harris AJ, Vaughan B, Yeomans JA, Smith PA, Burnage ST. Surface preparation of silicon carbide for improved adhesive bond strength in armour applications. Journal of the European Ceramic Society 2013;33:2925-2934.

[17] Tanoglu M, McKnight SH, Palmese GR, Gillespie JW, Use of silane coupling agents to enhance the performance of adhesively bonded alumina to resin hybrid composites. International Journal of Adhesion and Adhesives 1998;18:431-434.

[18] Rodrigues DD, Broughton JG. Silane surface modification of boron carbide in epoxy composites. International Journal of Adhesion and Adhesives 2013;46:62-73.

[19] Buchwalter LP, Oh TS, Kim J. Adhesion of polyimides to ceramics - effects of aminopropyltriethoxysilane and temperature and humidity exposure on adhesion. Journal of Adhesion Science and Technology 1991;5333-343.

[20] Blatz MB, Sadan A, Kern M. Resin-ceramic bonding: a review of the literature. The Journal of Prosthetic Dentistry 2003;89:268-274.

[21] Harris AJ, Yeomans JA, Smith PA, Vaughan B, Burnage ST. Surface treatment of alumina and silicon carbide for improved adhesive bond strength in armour. Presented at the 38th International Conference and Exposition on Advanced Ceramics and Composites. Daytona Beach: 2014.

[22] Wang XZ, Wang J, Wang H. Synthesis of a novel preceramic polymer (V-PMS) and its performance in heat-resistant organic adhesives for joining SiC ceramic. Journal of the European Ceramic Society 2012;32:3415-3422.

[23] Oh TS, Buchwalter LP, Kim J. Adhesion of polyimides to ceramic substrates - Role of acid-base interactions. Journal of Adhesion Science and Technology 1990;4:303-317.

[24] Moore DR. An introduction to the special issue on peel testing. International Journal of Adhesion and Adhesives 2008;28:153-157.

[25] Xie X, Karbhari VM. Peel test for characterization of polymer composite concrete interface. Journal of Composite Materials 1997;31:1806-1825.

[26] Karbhari VM, Engineer M. Investigation of bond between concrete and composites: use of a peel test. Journal of Reinforced Plastics and Composites 1996;15:208-227.

[27] de Freitas ST, Sinke J. Adhesion properties of bonded composite-to-aluminium joints using peel tests. Journal of Adhesion 2014;90:511-525.

[28] Moore DR, Williams JG. A protocol for the determination of the adhesive fracture toughness of flexible laminates by peel testing: fixed arm and T-peel methods. ESIS TC4 Test Protocol. London: Mechanical Engineering Department, Imperial College London; 2010. (http://www3.imperial.ac.uk/meadhesion/testprotocols/peel), (accessed 24/01/2013)

[29] Mehmood S, Madsen B. Properties and performance of flax yarn/thermoplastic polyester composites. Journal of Reinforced Plastics and Composites 2012;31:1746-1757.

[30] Pocius AV. Adhesion and adhesives technology: an introduction. Munich: Hanser Publishers; 1997.

[31] Digby RP, Shaw SJ. The international collaborative programme on organosilane coupling agents: an introduction. International Journal of Adhesion and Adhesives 1998;18:261-264.

[32] Johnsen BB, Olafsen K, Stori A. Reflection-absorption FT-IR studies of the specific interaction of amines and an epoxy adhesive with GPS treated aluminium surfaces. International Journal of Adhesion and Adhesives 2003;23:157-165.

[33] ISO 25178-2. Geometrical product specifications (GPS) - Surface texture: Areal, Part 2: Terms, definitions and surface texture parameters. International Organization for Standardization, Geneva; 2012.

[34] Guzman-Castillo ML, Bokhimi X, Rodriguez-Hernandez A, Toledo-Antonio A, Hernandez-Beltran F, Fripiat JJ. The surface energy of quasi-amorphous gamma-alumina calculated from the temperature of the gamma-alpha transition. Journal of Non-Crystalline Solids 2003;329:53-56.

[35] Joud JC, Vittoz C, Dubois PE. The van der Waals contribution to the surface energy of oxides. Proc. International Conference on High Temperature Capillarity. Cracow; 1997.

[36] Saga K, Hattori T. Identification and removal of trace organic contamination on silicon wafers stored in plastic boxes. Journal of the Electrochemical Society 1996;143:3279-3284.

[37] Bain CD, Whitesides GM, Depth sensitivity of wetting: monolayers of w-mercapto ethers on gold, Journal of the American Chemical Society 1988;110:5897-5898.

[38] Gledhill RA, Kinloch AJ, Yamini S, Young RJ. Relationship between mechanical properties of and crack propagation in epoxy resin adhesives. Polymer 1978;19:574-582.

[39] Greenhalgh ES. Failure analysis and fractography of polymer composites. Cambridge: Woodhead Publishing Limited; 2009.

[40] Pinho ST, Robinson P, Iannucci L. Fracture toughness of the tensile and compressive fibre failure modes in laminated composites. Composites Science and Technology 2006;66:2069-2079.

[41] Huang XN, Hull D. Effects of fiber bridging on Gic of a unidirectional glass epoxy composite. Composites Science and Technology 1989;35:283-299.

[42] Hu XZ, Mai YW. Mode-I delamination and fiber bridging in carbon-fiber epoxy composites with and without PVAL coating. Composites Science and Technology 1993;46:147-156.

[43] Abel ML, Digby RP, Fletcher IW, Watts JF. Evidence of specific interaction between gamma-glycidoxypropyltrimethoxysilane and oxidized aluminium using high-mass resolution ToF-SIMS. Surface and Interface Analysis 2000;29:115-125.

[44] Rattana A, Hermes JD, Abel ML, Watts JF. The interaction of a commercial dry film adhesive with aluminium and organosilane treated aluminium surfaces: a study by XPS and ToF-SIMS. International Journal of Adhesion and Adhesives 2002;22:205-218.

[45] Luciani A, Champagne MF, Utracki LA. Interfacial tension in polymer blends. 1. Theory. Polymer Networks & Blends 1996;6:41-50.

[46] Iyengar Y, Erickson DE. Role of adhesive-substrate compatibility in adhesion. J. Appl. Polym. Sci. 1967;11:2311-2324.